HHS Public Access

Author manuscript

Dev Biol. Author manuscript; available in PMC 2016 September 15.

Published in final edited form as:

Dev Biol. 2015 September 15; 405(2): 291–303. doi:10.1016/j.ydbio.2015.06.007.

Budgett's frog (*Lepidobatrachus laevis*): a new amphibian embryo for developmental biology

Nirav M. Amin[1], **Mandy Womble**[1], **Cris Ledon-Rettig**[2], **Margaret Hull**[1], **Amanda Dickinson**[3], and **Nanette Nascone-Yoder**[1,*]

[1]Department of Molecular Biomedical Sciences, 1060 William Moore Drive, College of Veterinary Medicine, North Carolina State University, Raleigh, NC, 27607 USA

[2]Department of Biology, Indiana University, 915 E. Third St. Bloomington, IN 47405

[3]Biology Department, Virginia Commonwealth University, 1000 W. Cary St. Richmond, VA 23284

Abstract

The large size and rapid development of amphibian embryos has facilitated ground-breaking discoveries in developmental biology. Here, we describe the embryogenesis of the Budgett's frog (*Lepidobatrachus laevis*), an unusual species with eggs that are over twice the diameter of laboratory *Xenopus*, and embryos that can tolerate higher temperatures to develop into a tadpole four times more rapidly. In addition to detailing their early development, we demonstrate that, like *Xenopus*, these embryos are amenable to explant culture assays and can express exogenous transcripts in a tissue-specific manner. Moreover, the steep developmental trajectory and large scale of *Lepidobatrachus* make it exceptionally well-suited for morphogenesis research. For example, the developing organs of the Budgett's frog are massive compared to those of most model species, and are composed of larger individual cells, thereby affording increased subcellular resolution of early vertebrate organogenesis. Furthermore, we found that complete limb regeneration, which typically requires months to achieve in most vertebrate models, occurs in a matter of days in the Budgett's tadpole, which substantially accelerates the pace of experimentation. Thus, the unusual combination of the greater size and speed of the Budgett's frog model provides inimitable advantages for developmental studies—and a novel inroad to address the mechanisms of spatiotemporal scaling during evolution.

Keywords

Lepidobatrachus; *Xenopus*; amphibian; embryo; stages; scaling

[*]Author for correspondence. phone: (919) 513-8284 (nmnascon@ncsu.edu).

Introduction

Amphibians have historically been ideal model organisms for experimental embryology because their relatively large, rapidly-developing embryos are abundant and highly accessible to microsurgical manipulations. Indeed, classical experiments on frog and salamander embryos profoundly influenced our current understanding of fundamental events in vertebrate development (Spemann and Mangold, 1924). In the twentieth century, the frog *Xenopus laevis* ascended as the amphibian of choice for modern embryologists, largely because of its responsiveness to year-round, hormone-induced ovulation in the laboratory (Callery, 2006). *Xenopus* explant assays transformed our conception of multi-potency and the cell behaviors that drive morphogenesis (Logan and Mohun, 1993; Saint-Jeannet et al., 1994; Sater and Jacobson, 1989; Wilson et al., 1989), while the capacity to microinject single blastomeres with molecular reagents continues to serve as a powerful system for tissue-specific analyses of gene function and the elucidation of regulatory networks (Amaya et al., 1991; Hopwood and Gurdon, 1990; Moody, 1987a; Moody, 1987b; Smith et al., 1993; Tandon et al., 2012; Woodland and Jones, 1987). In more recent years, genome resources have become available for *X. laevis* and its genetically tractable cousin, *X. tropicalis* (Hellsten et al., 2010). Consequently, even more sophisticated technologies continue to be added to the amphibian toolbox, including transgenic approaches (Hamlet et al., 2006; Kroll and Amaya, 1996; Ogino et al., 2006; Yergeau et al., 2009), targeted mutagenesis/genome editing via zinc finger nucleases, TALENs, and CRISPRs, and transcriptomic and proteomic profiling (Amin et al., 2014; Blitz et al., 2013; Guo et al., 2014; Lei et al., 2012; Liu et al., 2014; Nakajima and Yaoita, 2013; Nakayama et al., 2013; Rao et al., 2014; Sakane et al., 2014; Sun et al., 2014; Suzuki et al., 2013; Wuhr et al., 2014; Young et al., 2011)

In addition to *Xenopus*, and a few other species whose embryology has been described by evolutionary developmental biologists (del Pino et al., 2004; del Pino et al., 2007; Moya et al., 2007; Perez et al., 2009; Romero-Carvajal et al., 2009), there are about 6,500 other recorded species of frogs and toads with tremendous diversity, but there is almost no information on their development (AmphibiaWeb, 2014). Ironically, as one of the most highly derived genera, *Xenopus* is arguably not representative of most anurans (Hall, 1992). Given that hundreds of frogs are now threatened with extinction (Stuart et al., 2004), it is imperative that the biodiversity of amphibian embryogenesis be more fully assessed, not only to inform conservation efforts, but also because many species may be uniquely suited for illuminating critical issues at the interface of development, ecology and evolution (Calboli et al., 2011). For example, the amazing capacity of urodele amphibians to regrow multiple adult organs and tissue types has long been utilized as a system in which to illuminate the mechanisms of regeneration (Brockes and Kumar, 2002). Likewise, studying the distinct ontogeny of direct-developing frogs (e.g., *Eleutherodactylus*) has provided insight into the evolutionary origins of the amniote egg during the rise of terrestrial vertebrates (Elinson and Beckham, 2002). Finally, the exceptional developmental plasticity of Spadefoot toad tadpoles (e.g., *Spea*) has served as a striking example of the dynamic interplay between the environment and the genome in the manifestation of phenotype (Ledon-Rettig and Pfennig, 2011). In the context of technological advances that now facilitate “omic”-era approaches and enable genome editing in such species (Fei et al., 2014;

Flowers et al., 2014; Khattak et al., 2014; Sobkow et al., 2006; Whited et al., 2012), the time is ripe to redouble efforts to leverage the unique biology of additional frogs.

One intriguing candidate species is *Lepidobatrachus laevis* (known in the pet trade as "Budgett's frog"), a robust aquatic frog that lives in the Chaco region of South America (Budgett, 1899). *L. laevis* adults have enormous mouths and are aggressive and cannibalistic predators (Hanken, 1993; Fabrezi and Lobo, 2009; Ruibal and Thomas, 1988). The larvae of *L. laevis* have been studied because they progress extremely rapidly through metamorphosis, and exhibit an unusual feeding strategy for anuran tadpoles: obligate carnivory (Bloom et al., 2013; Fabrezi, 2006; Parker, 1931; Ruibal and Thomas, 1988; Ziermann et al. 2013; Hanken 1993). *L. laevis* larvae consume live prey, including other tadpoles, whole; the craniofacial and digestive tract specializations associated with this megalophagic (and often cannibalistic) feeding ecology have made *L. laevis* larvae captivating subjects for evolutionary biologists (Bloom et al., 2013; Carroll et al., 1991; Fabrezi, 2006; Hanken, 1993; Parker, 1931; Ruibal and Thomas, 1988; Ziermann et al., 2013), but the pre-feeding stages of *L. laevis* development have not yet been formally described.

Here, we document key stages in the early pre-feeding embryogenesis of *L. laevis* and demonstrate, through the application of standard methodologies, that they also possess the experimental amenability that has made *Xenopus* embryos so valuable. We provide evidence that the more expedient oocyte size and thermal tolerance of *L. laevis* provides practical advantages over existing vertebrate embryo models, including enhanced resolution of early organogenesis, and an accelerated time frame for regeneration. We posit that the unusual combination of "extreme" features in *L. laevis* could provide a novel inroad to address the cellular and molecular mechanisms that influence the pace and scale of morphogenesis during evolution.

Materials & Methods

Lepidobatrachus laevis embryo collection

Adult *L. laevis* frogs were obtained through the pet trade (Backwater Reptiles), and housed in de-chlorinated tap water at 28°C in individual tanks (to avoid cannibalism within the adult colony). Embryos were produced by natural matings between hormonally-induced male and female frogs; breeding pairs were size-matched to minimize potential aggression. Briefly, ovulation was induced by injection of 50 μg luteinizing hormone (LHRH; Sigma L7134) into the dorsal lymph sac of the female frog. Two hours later, 30 μg LHRH was injected into the dorsal lymph sac of the male. The male was then placed immediately into a 10 gallon mating tank, followed by the larger female (to discourage cannibalism), and the tank was covered with a dark towel. Amplexus was typically observed within one to two hours of placing the male and female together, and ovulation usually commenced within four hours of injecting the female with LHRH. In tanks with amplexing pairs, the fertilized eggs were collected periodically over a 4 hour period.

Fertilized embryos were carefully sorted and rinsed in 10% Holtfreter's solution (5.9 mM NaCl, 67 μM KCl, 76 μm $CaCl_2$, 240 μM $NaHCO_3$), then transferred to 10 cm petri plates containing fresh 10% Holtfreter's at 28°C. To avoid overcrowding and promote uniform

development, embryos were cultured at a density of <30 embryos per 100 mm plate. Embryos were staged according to standard amphibian staging criteria (Gosner, 1960).

To monitor embryonic development at different temperatures, fertilized *X. laevis* and *L. laevis* embryos were collected at the 2-cell stage and sorted into dishes of 10% Holtfreter's solution, which were incubated at five different temperatures (16°C, 23°C, 28°C, 32°C, 37°C). For this analysis, 20 *X. laevis* and 10 *L. laevis* embryos were scored for viability and growth rate at each temperature. Time-lapse imaging of *X. laevis* and *L. laevis* embryos was performed on a Zeiss SteREO Lumar.V12 with AxioVision and compiled into movies using ImageJ software, version 1.45S (NIH).

Animal cap assays

L. laevis animal caps were dissected at Gosner stage 8–8.5 (Gosner, 1960) using sharpened Watchmaker's forceps, and cultured at 28°C in 2 mL of 2 ng/ml human activin A (R&D Systems) in 0.75X MMR (75 mM NaCl, 1.5 mM KCl, 0.75 mM $MgSO_4$, 1.5 mM CaCl2, 3.75 mM HEPES, 75 μM EDTA, pH 7.8) for 14 hours in agarose coated wells of a 24-well plate. Untreated caps were used as controls. For comparison, *X. laevis* caps were also dissected and cultured in the presence or absence of 2 ng/ml activin, as previously described (Dush et al., 2011). Caps were fixed in 4% paraformaldehyde (PFA) and imaged at 14 hours post dissection.

Microinjection

L. laevis embryos from natural matings were de-jellied manually, or incubated for 5–7 minutes in 2% cysteine hydrochloride (pH 7.8–8.1), and microinjected at the indicated stages. Injections were performed in 3% Ficoll dissolved in 10% Holtfreter's solution. The mMessage transcription kit (Ambion) was used to generate capped mRNA for eGFP (120 pg/nl), which was combined with 2 ng/nl fluorescent dextran-(Alexa555), and back-loaded into pulled, calibrated glass pipettes (Sive et al., 1998); 2 nl of this mixture was injected at the stages described. Embryos were allowed to recover in 3% Ficoll for 20 minutes, and then transferred to individual wells of a 12-well plate containing 10% Holtfreter's solution for longer term incubation. Fluorescence was imaged at 48 hpf using a Zeiss SteREO Lumar.V12 with AxioVision.

Immunostaining

Immunohistochemical staining was performed as previously described for *Xenopus* (Dush, 2011). Whole embryos were fixed with eight consecutive washes of Dent's Fixative (80% Methanol, 20% DMSO) and stored overnight at −20°C. Embryos were rinsed three times with PBST before transfer to sucrose/gelatin (15% sucrose/25% cold water fish gelatin) and stored overnight at room temperature. Embryos were embedded in OCT (Tissue-Tek), sectioned at 10 μm using a Leica CM 1850 cryostat and mounted on coated slides (Fisher Superfrost). Sections were post-fixed for two minutes in 4% PFA [100 mM Hepes (pH 7.4), 100 mM NaCl, 4% paraformaldehyde] and blocked for 30 minutes as previously described (Reed, 2009). Antibodies were applied overnight at 4°C in an antibody amplifier humidity chamber (Prohisto). Dilutions of primary antibodies used are as follows: anti-β-catenin (Santa Cruz, sc-7199, 1:100), anti-γ-tubulin (abcam, ab270714, 1:1000), anti-α-tubulin

(Sigma, T9026, 1:1000), and anti-F-actin (Cytoskeleton, AAN01, 1:200). Slides were then washed three times in PBST for 5 minutes, incubated for 3 hours in blocking buffer containing Alexa 488-conjugated goat anti-mouse IgG (Invitrogen, A11029; 1:2000) and/or Alexa 546-conjugated goat anti-rabbit IgG (Invitrogen, A11035; 1:2000). To stain nuclei, sections were washed twice in PBST, twice with PBS and incubated for 5 minutes in PBS containing TO-PRO-3 (Invitrogen, T3605, 1:1000). Stained slides were washed twice with PBS and mounted with coverslips and ProLong Gold Antifade Reagent (Invitrogen) before imaging on a Leica (Model TCS-SPE) confocal microscope. Maximum projections of z-stacks are shown.

Limb Regeneration

Tadpoles (48 hpf) were maintained in large tanks and fed on siblings *ad libitum*. Individual tadpoles were anesthetized by immersion in 0.05% tricaine methanesulfonate (MS-222). Once anesthetized, the right limb was amputated just distal to the geniculate joint in a straight line with sharp iridectomy scissors (Dent, 1962; Goode, 1967). The tadpole was monitored for hemostasis before anesthetic recovery. Operated tadpoles were then cultured individually and fed *Xenopus* tadpoles. Regenerating limbs were imaged on a Zeiss SteREO Lumar.V12 with AxioVision every 24 hours for at least three weeks.

Results

Lepidobatrachus laevis developmental staging

Below, we include an account of normal *L. laevis* development, with a focus on the critical phases of early ontogeny (cleavage, gastrulation, neurulation and organogenesis), as compared with *Xenopus laevis*. We have chosen to describe *L. laevis* normal development at 28°C, a temperature that falls within the overlap of the published ranges of thermal tolerance of embryos, larvae and adults of this species (Carroll, 1996). As *X. laevis* embryos do not survive at this temperature (Khokha et al., 2002), Figure 1 compares the schedule of *L. laevis* development at 28°C with that of *X. laevis* embryos raised at 23°C, as described in the widely-used normal table of *X. laevis* development (Nieuwkoop and Faber, 1994); however, it should be noted that *L. laevis* and *X. laevis* develop at the same rate when raised at mutually permissive temperatures (e.g., 23°C; see Figure 5).

Cleavage

The *L. laevis* egg (Figure 2A) is relatively large (~2.6 mm) compared to that of *X. laevis* (~1.2 mm). Nonetheless, the early *L. laevis* embryo appears to undergo holoblastic cleavage (albeit with larger vegetal than animal blastomeres), and requires only 15–20 minutes between divisions. The orientation of cleavage planes is analogous to *X. laevis* (Figure 2B–E) and largely synchronous among different individuals through the 32-cell stage, i.e., Gosner (GS) stages 1–7, after which the orientation of these divisions is less uniform. *L. laevis* embryos reach mid-cleavage stage within 4 hours post fertilization (hpf, Figure 2F) and most reach late blastula stages by 5–6 hpf (Figure 2G–H). Thus, despite the increased size of the egg in *L. laevis* (see Figure 2I), cleavage can still occur rapidly.

Gastrulation

Gastrulation commences in *L. laevis* with the appearance of an arc of pigmentation demarcating the involuting dorsal lip at GS10 (Figure 2J). The arc then expands circumferentially to form a complete circle delimiting the yolk plug and future blastopore at GS11 (Figure 2K). These events are reminiscent of initial gastrulation in *Xenopus* species. However, whereas in *Xenopus* the entire vegetal endoderm is gradually subsumed into the interior of the embryo, the endoderm mass of *L. laevis* embryos remains slightly protuberant during gastrulation (Figure 2L). Interestingly, despite the substantially larger diameter and potential physical hindrance of this protruding yolk plug, blastopore closure ensues rapidly and is complete by 10 hpf (see Figure 3A).

Neurulation and Organogenesis

During neurulation, *L. laevis* forms a broad, keyhole-shaped neural plate (Figure 3A). Despite the larger scale, subsequent formation of neural folds (Figure 3B) and closure of the neural tube (Figure 3C) takes only ~6hrs (GS13-GS16), and migratory streams of neural crest in the prospective pharyngeal arches become obvious even before the neural tube is closed, as early as ~12hpf (G14; see arrows, Figure 3B). These detailed features of neural tube development are highly discernable in *L. laevis* (Supplemental Movie 1). Upon neural tube closure (~16hpf), the somites become visible (see Figure 3C). The embryo immediately begins elongating along the anterior-posterior axis (Figure 3D–E) and “hatches” out of the surrounding thick jelly layers. At this stage, the embryo begins to exhibit a motor response to external stimuli.

The formation of the major craniofacial structures, including the cement gland, eyes, nasal pit and gill buds, begins within a few hours of neural tube closure (Figures 3D–H, 4). Initially, the pharyngeal arches appear as protruding pouches at GS17-18 (18–20 hpf; Figure 4A–B), which form external gill buds a few hours later (Figure 4D–E), and then quickly undergo branching morphogenesis to form elaborate gills by 28 hpf (Figures 3F–H, 4G–K). Along with the pharyngeal arches, the stomodeum becomes obvious as a dorsoventally elongated invagination at the midline of the face (Figure 4). By 28 hpf, the buccopharyngeal membrane has already perforated (see Figure 4H–I) to allow the embryonic mouth to be connected to the foregut. By GS20, the nasal pits have formed (Figure 4D), and by GS21 (27 hpf), the optic cup has expanded into a horseshoe shape with an evident lens (Figure 4G). We note that the *L. laevis* craniofacial structures are substantially larger and more prominent than in *X. laevis*. Indeed, individual cells in the face are readily apparent under only a dissecting microscope (e.g., see Figure 4C,F,I,L).

Along with craniofacial morphogenesis, other organogenesis events also commence shortly after neurulation in *L. laevis*. The pronephros is evident immediately following neural tube closure (Figures 3D–F). Heartbeat commences before the end of the first day (~21 hpf; GS19), with looping and septation complete by ~24hpf, and functional blood circulation visible in the gills and fins by 27–28 hpf (GS20-22; not shown). Morphogenesis of the digestive tract is also evident before the end of the first day (Figure 3H), with overt gut looping and pre-feeding intestinal lengthening concluded by ~36–40 hpf [not shown, but see Bloom et al., 2013]. *L. laevis* tadpoles have been observed to begin feeding on their siblings

as early as 48 hpf, indicating that the gut is fully functional by two days post fertilization at 28°C. Thus, despite the larger size, organogenesis proceeds at a rapid rate in the *L. laevis* embryo.

L. laevis embryos can tolerate a wide range of temperatures

The ability to accelerate or decelerate the developmental trajectory of laboratory *Xenopus* embryos by shifting them to higher or lower temperatures, respectively, has enabled experimental manipulation of any stage of development at convenient times of the day. However, at temperatures outside of a species-specific optimal range, accelerated or decelerated embryos display developmental defects and decreased viability (Khokha et al., 2002). Although *L. laevis* embryos and larvae have been reported to enjoy a broad range of thermal tolerance (Carroll, 1996), the morbidity of embryos grown at different temperatures in the laboratory has not been explicitly described.

To determine the optimal temperature range for normal morphological development of *L. laevis*, we raised *L. laevis* and *X. laevis* embryos in parallel at temperatures ranging from 16°C to 37°C. At the lowest temperature tested (16°C), *X. laevis* embryos developed normally, while all the *L. laevis* embryos failed to complete gastrulation. However, at 23°C, the embryos of both species developed with normal morphology and, despite their size difference, at a similar pace (Figure 5; Supplemental Movie 2). This suggests that the lower temperature limit for *L. laevis* development is between 16°C and 23°C.

At 28°C, both species cleaved at a similar rate. However, the majority of the *X. laevis* embryos (55%; n=20) failed to gastrulate and the remainder developed severe ventral edemas by GS17, indicating that the upper temperature limit of *X. laevis* development is below 28°C, consistent with previous results (Khokha et al, 2002). In contrast, all *L. laevis* embryos developed normally at 28°C, as expected. Moreover, *L. laevis* embryos continued to thrive at temperatures that cause all *X. laevis* embryos to die before completing gastrulation (32°C and 37°C; Figure 5). Strikingly, *L. laevis* develops at a dramatically accelerated pace at 37°C, reaching feeding tadpole stages in less than a day—about four times as fast as *X. laevis* raised at 23°C—with no obvious defects in development. Overall, these results demonstrate that, like *Xenopus* species, *L. laevis* is amenable to temperature-mediated manipulation of developmental rate for experimenter convenience.

L. laevis enables lineage tracing in live embryos at high resolution and accuracy

Xenopus blastulae often exhibit patterns of cleavage and pigmentation that enable specific lineages to be targeted for microinjection. For example, future ventral blastomeres can often be identified by their darker pigmentation and slightly larger size in comparison to the lighter and slightly smaller dorsal blastomeres (Moody, 1987a; see Figure 2D–E). *Lepidobatrachus* blastulae exhibit similar dorsal-ventral asymmetries and apparent holoblastic cleavage. However, in other frog species with large eggs, it has been found that germ layer positions, and thus blastomere fate maps, may be altered (i.e., shifted along the animal-vegetal axis), or that the early cleavage divisions remain incomplete (Elinson and Beckham, 2002; Moya et al., 2007). If such features exist in *L. laevis*, this would limit the utility of this species for lineage-specific assays.

To determine whether specific tissues can be reliably targeted by microinjection in *L. laevis*, we microinjected fluorescent dextran into one blastomere of a *L. laevis* embryo at the 2-cell stage. In *Xenopus* species, the first cleavage generally corresponds to the embryonic midline; thus, injecting one cell at the 2-cell stage results in mostly unilateral localization of the fluorescent lineage tracer to either the left or right side of the embryo (Ramsdell et al., 2006). Likewise, in *L. laevis*, this injection resulted in robust fluorescence limited predominantly to one side of the animal (Figure 6A–B). Thus, despite their larger scale, the first cleavage plane also corresponds generally with the axial midline of *L. laevis*.

To ascertain whether fate maps of later stage *X. laevis* blastomeres (e.g., at the 16–32-cell stage) could also be used to target specific tissues in *L. laevis*, we microinjected fluorescent dextran into analogous later stage blastomeres in *L. laevis*. These injections yielded a similar distribution of the fluorescent label in *L. laevis* as previously reported in *Xenopus*, with high reproducibility (Figure 6D–F; 75% targeting the foregut, n=8). Moreover, we found that *L. laevis* blastomeres are easily injectable up to at least the 128-cell stage (Figure 6G–I), potentially allowing lineage tracing of later stage fates and, thus, finer targeting of more discrete tissues in the larger embryo. Importantly, co-injection of synthetic capped mRNA encoding eGFP resulted in strong green fluorescence in the progeny of the injected blastomeres (Figure 6C). These results show that *L. laevis* embryos are not only amenable to fate mapping studies with lineage tracers, but are also able to express exogenous mRNA for highly targeted gain of function studies.

L. laevis animal caps respond to external stimuli similarly to *Xenopus*

A key technical advantage of amphibian embryos is the ability to culture explants of embryonic tissues *in vitro* (Logan and Mohun, 1993; Saint-Jeannet et al., 1994; Sater and Jacobson, 1989; Sater and Jacobson, 1990; Wilson et al., 1989; Woodland and Jones, 1987). *X. laevis* has long been exploited for the “animal cap” assay, in which a disc of naïve ectoderm tissue from the animal pole of the GS8-9 embryo is induced to form an alternate fate (e.g., mesoderm) by culturing it in the presence of biologically active molecules, such as the TGF-β ligand, activin. An easily observable readout of the induction of mesoderm is the elongation of the isolated tissue (which normally forms a ball of ciliated epidermis *in vitro*), reflecting the convergent extension rearrangements that are executed by axial/paraxial mesoderm during gastrulation (compare Figures 7A and C; Brieher and Gumbiner, 1994; Dush et al., 2011; Smith et al., 1990). However, considering the more sizeable dimensions of the ectoderm in *L. laevis*, and the potential for accelerated execution of its morphogenetic processes, it is unclear how Budgett’s frog animal caps might respond to *in vitro* explant culture.

To test this response, we dissected animal caps from GS8-9 embryos and cultured them in the presence or absence of 2ng/ml activin. Although animal caps from the *L. laevis* embryo are equivalent in diameter to an entire *X. laevis* blastula (but smaller caps may be cultured, e.g., rightmost cap in Figure 7B), they nonetheless quickly heal into spherical shapes that eventually differentiate into ciliated epidermis (Figure 7B), similar to untreated *X. laevis* caps. Moreover, when exposed to activin, these explants rapidly undergo obvious

convergent extension (Figure 7D). Thus, as in *X. laevis*, *L. laevis* tissues are highly amenable to explant assays.

A high resolution view of organ development in *L. laevis*

Because *L. laevis* embryos are considerably bigger than *X. laevis*, they provide outstanding resolution of the emergence of gross morphology, such as neural folds and craniofacial features. However, they also possess relatively enormous internal organs. For example, at ~0.6 mm in length, the early *Lepidobatrachus* heart tube is almost as long as an entire neurula stage *X. laevis* embryo (Figure 8A). Likewise, the looped heart of a *L. laevis* tadpole is substantially larger than a comparable stage *X. laevis* heart (Figure 8B). These observations suggest that the increased scale of *L. laevis* organs could provide greater cellular resolution of organogenesis events than *X. laevis*.

To assess this possibility, we characterized tissue architecture during *L. laevis* heart morphogenesis by applying a panel of antibodies known to detect *Xenopus* proteins, including markers of cell-cell adhesion (β-catenin) and the cytoskeleton (α/γ-tubulin, actin) (Figure 8C–J). We note that, with the increased scale of the larger embryo, a cross section of only the heart of *L. laevis* is approximately the same size as an entire *Xenopus* embryo (100x magnification; compare Figure 8C and D). Consequently, the distinction between the myocardial and endocardial tissue layers, including individual cell shapes, is more evident in *L. laevis* heart sections at low magnification (compare Figure 8C and D).

Interestingly, comparing the dimensions of individual cells in *L. laevis* and *X. laevis* hearts at a similar stage of cardiogenesis revealed that differentiating cells in the *L. laevis* organ are actually about 50% larger (1.46X, $p<0.001$ for myocardium; 1.47X, $p<0.0001$ for endocardium) than those that comprise a comparable stage *X. laevis* heart. Fortuitously, this increase in cell size enables discernment of subcellular organization in the endocardial versus myocardial layers at even early heart tube stages (Figure 8H–J). For example, standard confocal microscopy at only moderately high (400X) magnification can be used to visualize the orientation of microtubule architecture (Figure 8G–H), the position of centrioles (Figure 8I–J), the apical enrichment of adherens junction components (Figure 8G–H) and the polarization and alignment of bundles of actin filaments (Figure 8I–J). Thus, the inherently greater cell size of *L. laevis* embryonic organs yields exceptional resolution of very early stages of vertebrate organogenesis.

Limb Regeneration in *L. laevis* occurs rapidly

Given the rapid development attainable in *L. laevis*, we reasoned that the process of regeneration might also be accelerated. However, not all frogs show regenerative capacity (Scadding, 1977). To test if *L. laevis* would be an appropriate frog model for accelerated regeneration studies, we amputated the hindlimb of *L. laevis* tadpoles at a stage of limb development comparable to that typically used in *X. laevis* (8 dpf; Figure 9A; Beck, 2012). By 24 hours, a blastema was visible (Figure 9B), and a fully regenerated limb (Figure 9C) was observed less than 10 days post-amputation (80%; $n=5$). Notably, by 21 days post amputation, the regenerated *L. laevis* limb was indistinguishable from the unoperated limb

in both pattern and size (data not shown)—this can take months to achieve in other species, such as axolotl (Goode, 1967; Tank et al., 1976; Young et al., 1983).

In *Xenopus* and other frogs, regeneration capacity diminishes as tadpoles approach metamorphosis (Dent, 1962). *L. laevis* also possesses this plasticity, as amputations performed a few days later (12 dpf) result in partial regeneration, 2.33±0.58 digits; *n*=3). Moreover, amputations performed at 14 dpf result in only a single spike (n=2; data not shown). This fortuitous plasticity allows investigation of the differences between regenerative and non-regenerative limbs (Yokoyama et al., 2011). Thus, *L. laevis* can serve as an accelerated model of all aspects of tadpole limb regeneration.

Discussion

Here, we describe the normal embryogenesis and experimental amenability of the Budgett's Frog (*Lepidobatrachus laevis*). Although we previously showed that *L. laevis* embryos are receptive to RNA *in situ* hybridization and pharmacological manipulation of signaling pathways (Bloom et al., 2013), their utility for classical experimental manipulation was untested. In this study, we assayed the responsiveness of the *L. laevis* embryo to microinjection, explant culture, immunohistochemical staining and regeneration, as proof of principle of its potential to serve as a complementary amphibian system. Moreover, the unusual combination of large size and rapid embryogenesis in this species make it a powerful developmental model in its own right, particularly when an increase in the resolution or speed of morphogenesis is desired.

Size matters: Benefits of larger amphibian embryos

Most amphibian eggs undergo holoblastic cleavage; however, eggs greater than ~2 mm in diameter can exhibit altered cleavage patterns, such as partially meroblastic divisions (Collazo and Keller, 2010; del Pino and Loor-Vela, 1990; Elinson and Beckham, 2002). Likewise, while most small eggs completely internalize the vegetal yolk mass during gastrulation/epiboly, in some larger (3.5 mm) eggs (e.g., *E. coqui*), the yolk mass cannot be completely subsumed by epiboly and must be secondarily covered after gastrulation by the ventral-ward expansion of tissue from the body wall (Elinson and Beckham, 2002). Our observations indicate that, despite their relatively large size, *L. laevis* embryos are still able to undergo the ancestral mode of holoblastic cleavage and completely internalize the yolk mass by epiboly. Thus, at ~2.6 mm in diameter, the *L. laevis* embryo appears to have achieved maximal enlargement while still retaining an early developmental program that is comparable to ancestral anurans.

From a pragmatic perspective, the increased scale of *Lepidobatrachus* embryos enables facile injection of single blastomeres up to at least the 128-cell stage and poses the prospect of high resolution fate mapping or extremely localized gain-of-function strategies. The morphology of developing structures, such as craniofacial features, is inherently magnified, allowing easier visualization and tracking of the fine details of morphogenesis. Structures such as the pharyngeal arches, stomodeum, gill buds, and embryonic mouth are larger and more prominent than in *X. laevis*, which could enhance studies of craniofacial development. Indeed, under a simple dissecting microscope, individual cells in the face of *L. laevis* are

apparent; this resolution could facilitate cell fate and migration studies. In addition, tissues of interest may be more accurately isolated in the larger embryo, opening the possibility of fine-scale explant culture or transplantation experiments. Finally, the substantial (~50%) enlargement of the individual cells themselves affords views of the cellular architecture of early organs that, to our knowledge, are not otherwise attainable without advanced microscopy or special imaging modalities. Fortuitously, many antibodies known to detect *Xenopus* proteins also tend to be efficacious in *L. laevis*. Combined with the ability to express exogenous fluorescently-tagged proteins, the amplified scale of *L. laevis* cells and tissues has the potential to yield spectacular resolution of the cell biology underlying morphogenesis.

Perhaps an application in which the distinctive size of *L. laevis* will be particularly profitable is as a source of embryonic tissues for transcriptomic and/or proteomic profiling of highly discrete developmental events. *Xenopus* embryos have been shown to offer distinct advantages for proteomic analyses because of the relatively large amounts of material available (Amin et al., 2014; Rao et al., 2014; Sun et al., 2014; Wuhr et al., 2014). It is reasonable to assume that the even larger size of *L. laevis* could enable isolation of sufficient protein from sub-regions of organ anlage or key zones of morphogenetic activity. Although the *L. laevis* genome still awaits sequencing, genome-independent proteomic strategies have recently been shown to be feasible for non-model species (Wuhr et al., 2014). Since *L. laevis* is a diploid organism (Faivovich et al., 2014), sequencing and assembly of its genomic sequence should be less cumbersome than for the pseudotetraploid *X. laevis*. Moreover, a draft transcriptome assembly from embryonic organs contains greater than 26,000 predicted *L. laevis* proteins [including over 10,000 full-length ORFs with significant similarity to human proteins (BLAST *e*value of less than $10^{-5;}$ N.M.A., N.N.-Y.-unpublished data)]; thus, what we learn in this large-egged cannibalistic frog has great potential to provide insight into bio-medically relevant biology.

The need for speed: rapid development, rapid results

Despite the sizeable mass of the *L. laevis* embryo compared to *X. laevis*, its cleavage and development to tadpole proceeds at a comparable rate at the same temperature. This is highly unexpected because, in most amphibians, larger egg size is accompanied by substantially slower development. For example, although frog embryos comparable in size to *L. laevis* (e.g., *G. riobambae* at ~3 mm, or the Dendrobatids at 2–3.5 mm) have been reported to require 14 days or longer to complete gastrulation (del Pino et al., 2007), this feat may be achieved in as few as ~9 hours in *L. laevis* raised at 28°C. In addition, the ability to dramatically accelerate *L. laevis* development by culturing at temperatures as high as 37°C will facilitate the study of later stage events that take days or weeks to complete in other vertebrate models. For example, digestive tract morphogenesis takes ~3.5–4 dpf in *X. laevis* (raised at 23°C), ~3 days in zebrafish, ~10 days in chicken, and >2 weeks in the mouse, but can be achieved in less than 24 hpf in *L. laevis* raised at 37°C. Likewise, the ability to culture *L. laevis* at lower temperatures to decelerate development will allow one to maximize the size advantage of the species for dissections or lineage tracing at precise developmental time points.

The steep developmental trajectory of *L. laevis* extends beyond embryogenesis. Currently, a major limitation of limb regeneration experiments is the extended time required to achieve full regeneration (Azevedo et al., 2011). However, we have shown that, in *L. laevis*, amputation may be initiated as early as 7–8 days after fertilization, with limb regeneration evident a little over a week (~10 days) post-amputation (at 28°C). Thus, a *complete* regeneration experiment, from fertilization to regrowth (~45 days in *Xenopus*) requires only ~2.5 weeks in *L. laevis*—and is likely to be further accelerated by higher rearing temperatures. The dramatically compressed timetable for organogenesis and regeneration at higher temperatures not only enables more experiments to be completed in less time, but may also facilitate high resolution imaging of events that typically occur over weeks or months in other species, a prohibitively long duration for standard time-lapse. Lastly, we note that, under ideal conditions of nutrition and temperature, *L. laevis* metamorphosis is complete in only a few weeks. Froglets exhibit adult size and evidence of sexual behavior in as few as 4 months, and yield F1 offspring in as few as 8 months (NNY, NA, unpublished observations); thus, expedient multi-generational studies involving mutant and/or transgenic lines may be a realistic possibility for this species.

Future Prospects: A model of biological scaling

Because of their impressive size and expeditious development, *L. laevis* embryos constitute a novel vertebrate system in which to investigate the poorly understood mechanisms of biological scaling, specifically, the impact of increased cell size and/or accelerated developmental rate on basic cellular processes and embryonic patterns. For example, how are the larger blastomeres in *L. laevis* able to properly distribute chromosomes, cytoplasmic determinants and organelles prior to cytokinesis in a time frame comparable to a much smaller embryo? How are intra- and extracellular signaling events regulated in order to maintain pattern invariance in the context of enlarged cells, expanded morphogenetic fields, and a hastened rate of organogenesis? Are the biomechanical forces and material properties that drive morphogenetic cell movements modified in larger embryos? How do different size embryos modulate cellular and molecular events to control the pace of cell division during morphogenesis? The answer to this latter question has implications for not only evolution, but also for the advancement of pathological events such as tumor progression. By serving as an extreme point of comparison to other anurans, the larger and faster Budgett's frog embryo may help us to understand, and ultimately predict, the phenotypic consequences of varying the fundamental physical parameters of metazoan development.

Supplementary Material

Refer to Web version on PubMed Central for supplementary material.

Acknowledgments

We would like to thank Dr. Michael Dush for suggestions on the manuscript, Dr. Michael Levy for his guidance in the husbandry of the animals used in this work, and Dr. Michael Levin for advice on regeneration experiments. This work was supported by NIH (RO1 DK085300, R21 OD017963) awards to N.N-Y.

References

Amaya E, Musci TJ, Kirschner MW. Expression of a dominant negative mutant of the FGF receptor disrupts mesoderm formation in *Xenopus* embryos. Cell. 1991; 66:257–270. [PubMed: 1649700]

Amin NM, Greco TM, Kuchenbrod LM, Rigney MM, Chung MI, Wallingford JB, Cristea IM, Conlon FL. Proteomic profiling of cardiac tissue by isolation of nuclei tagged in specific cell types (INTACT). Development. 2014; 141:962–73. [PubMed: 24496632]

AmphibiaWeb. Information on amphibian biology and conservation. Berkeley, California: AmphibiaWeb; Dec 15. 2014

Azevedo AS, Grotek B, Jacinto A, Weidinger G, Saude L. The regenerative capacity of the zebrafish caudal fin is not affected by repeated amputations. PLoS One. 2011; 6:e22820. [PubMed: 21829525]

Beck CW. Studying regeneration in *Xenopus*. Methods Mol Biol. 2012; 917:525–39. [PubMed: 22956108]

Blitz IL, Biesinger J, Xie X, Cho KW. Biallelic genome modification in F(0) *Xenopus tropicalis* embryos using the CRISPR/Cas system. Genesis. 2013; 51:827–834. [PubMed: 24123579]

Bloom S, Ledon-Rettig C, Infante C, Everly A, Hanken J, Nascone-Yoder N. Developmental origins of a novel gut morphology in frogs. Evolution & Development. 2013; 15:213–223. [PubMed: 23607305]

Brieher WM, Gumbiner BM. Regulation of C-cadherin function during activin induced morphogenesis of *Xenopus* animal caps. J Cell Biol. 1994; 126:519–527. [PubMed: 8034750]

Brockes JP, Kumar A. Plasticity and reprogramming of differentiated cells in amphibian regeneration. Nat Rev Mol Cell Biol. 2002; 3:566–574. [PubMed: 12154368]

Budgett JS. Notes on the batrachians of the Paraguayan Chaco, with observations upon their breeding habits and development, especially with regard to *Phyllomedusa hypochondrialis*, Cope. Also a description of a new genus. QJ Microsc Sci. 1899:305–333.

Calboli FC, Fisher MC, Garner TW, Jehle R. The need for jumpstarting amphibian genome projects. Trends Ecol Evol. 2011; 26:378–379. [PubMed: 21561678]

Callery EM. There's more than one frog in the pond: a survey of the Amphibia and their contributions to developmental biology. Semin Cell Dev Biol. 2006; 17:80–92. [PubMed: 16337414]

Carroll EJ. Thermal tolerance and heat shock protein synthesis during development in the anuran *Lepidobatrachus laevis*. Dev Growth Differ. 1996; 38:9–14.

Carroll EJ, Seneviratne AM, Ruibal R. Gastric Pepsin in an Anuran Larva. Dev Growth Differ. 1991; 33:499–507.

Collazo A, Keller R. Early development of *Ensatina eschscholtzii*: an amphibian with a large, yolky egg. Evodevo. 2010; 1:1. [PubMed: 20849644]

del Pino EM, Avila ME, Perez OD, Benitez MS, Alarcon I, Noboa V, Moya IM. Development of the dendrobatid frog *Colostethus machalilla*. Int J Dev Biol. 2004; 48:663–670. [PubMed: 15470639]

del Pino EM, Loor-Vela S. The pattern of early cleavage of the marsupial frog *Gastrotheca riobambae*. Development. 1990; 110:781–789. [PubMed: 2088720]

del Pino EM, Venegas-Ferrin M, Romero-Carvajal A, Montenegro-Larrea P, Saenz-Ponce N, Moya IM, Alarcon I, Sudou N, Yamamoto S, Taira M. A comparative analysis of frog early development. Proc Natl Acad Sci U S A. 2007; 104:11882–11888. [PubMed: 17606898]

Dent JN. Limb regeneration in larvae and metamorphosing individuals of the South African clawed toad. J Morphol. 1962; 110:61–77. [PubMed: 13885494]

Dush MK, McIver AL, Parr MA, Young DD, Fisher J, Newman DR, Sannes PL, Hauck ML, Deiters A, Nascone-Yoder N. Heterotaxin: a TGF-beta signaling inhibitor identified in a multi-phenotype profiling screen in *Xenopus* embryos. Chem Biol. 2011; 18:252–263. [PubMed: 21338922]

Elinson RP, Beckham Y. Development in frogs with large eggs and the origin of amniotes. Zoology (Jena). 2002; 105:105–117. [PubMed: 16351861]

Fabrezi M. Morphological evolution of Ceratophryinae (Anura, Neobatrachia). J Zool Sys Evol Res. 2006; 44:153–166.

Faivovich J, Nicoli L, Blotto BL, Pereyra MO, Baldo D, Barrionuevo JS, Fabrezi M, Wild ER, Haddad CFB. Big, Bad, and Beautiful: Phylogenetic Relationships of the Horned Frogs (Anura: Ceratophryidae). South Am J Herpetol. 2014; 9:207–227.

Fei JF, Schuez M, Tazaki A, Taniguchi Y, Roensch K, Tanaka EM. CRISPR-mediated genomic deletion of Sox2 in the axolotl shows a requirement in spinal cord neural stem cell amplification during tail regeneration. Stem Cell Reports. 2014; 3:444–459. [PubMed: 25241743]

Flowers GP, Timberlake AT, McLean KC, Monaghan JR, Crews CM. Highly efficient targeted mutagenesis in axolotl using Cas9 RNA-guided nuclease. Development. 2014; 141:2165–2171. [PubMed: 24764077]

Goode RP. The regeneration of limbs in adult anurans. J Embryol Exp Morphol. 1967; 18:259–267. [PubMed: 6059966]

Gosner KL. A simplified table for staging anuran embryos and larvae. Herpetologica. 1960

Guo X, Zhang T, Hu Z, Zhang Y, Shi Z, Wang Q, Cui Y, Wang F, Zhao H, Chen Y. Efficient RNA/Cas9-mediated genome editing in *Xenopus tropicalis*. Development. 2014; 141:707–714. [PubMed: 24401372]

Hall, BK. Evolutionary Developmental Biology. Chapman & Hall; 1992.

Hamlet MR, Yergeau DA, Kuliyev E, Takeda M, Taira M, Kawakami K, Mead PE. Tol2 transposon-mediated transgenesis in *Xenopus tropicalis*. Genesis. 2006; 44:438–445. [PubMed: 16906529]

Hanken J. Model Systems Versus Outgroups - Alternative Approaches to the Study of Head Development and Evolution. Amer Zool. 1993; 33:448–456.

Hellsten U, Harland RM, Gilchrist MJ, Hendrix D, Jurka J, Kapitonov V, Ovcharenko I, Putnam NH, Shu S, Taher L, et al. The genome of the Western clawed frog *Xenopus tropicalis*. Science. 2010; 328:633–636. [PubMed: 20431018]

Hopwood ND, Gurdon JB. Activation of muscle genes without myogenesis by ectopic expression of MyoD in frog embryo cells. Nature. 1990; 347:197–200. [PubMed: 1697650]

Khattak S, Murawala P, Andreas H, Kappert V, Schuez M, Sandoval-Guzman T, Crawford K, Tanaka EM. Optimized axolotl (*Ambystoma mexicanum*) husbandry, breeding, metamorphosis, transgenesis and tamoxifen-mediated recombination. Nat Protoc. 2014; 9:529–540. [PubMed: 24504478]

Khokha MK, Chung C, Bustamante EL, Gaw LW, Trott KA, Yeh J, Lim N, Lin JC, Taverner N, Amaya E, et al. Techniques and probes for the study of *Xenopus tropicalis* development. Dev Dyn. 2002; 225:499–510. [PubMed: 12454926]

Kroll KL, Amaya E. Transgenic *Xenopus* embryos from sperm nuclear transplantations reveal FGF signaling requirements during gastrulation. Development. 1996; 122:3173–3183. [PubMed: 8898230]

Ledon-Rettig CC, Pfennig DW. Emerging model systems in eco-evo-devo: the environmentally responsive spadefoot toad. Evol Dev. 2011; 13:391–400. [PubMed: 21740512]

Lei Y, Guo X, Liu Y, Cao Y, Deng Y, Chen X, Cheng CH, Dawid IB, Chen Y, Zhao H. Efficient targeted gene disruption in *Xenopus* embryos using engineered transcription activator-like effector nucleases (TALENs). Proc Natl Acad Sci U S A. 2012; 109:17484–17489. [PubMed: 23045671]

Liu Y, Luo D, Lei Y, Hu W, Zhao H, Cheng CH. A highly effective TALEN-mediated approach for targeted gene disruption in *Xenopus tropicalis* and zebrafish. Methods. 2014; 14:00041–00043.

Logan M, Mohun T. Induction of cardiac muscle differentiation in isolated animal pole explants of *Xenopus laevis* embryos. Development. 1993; 118:865–875. [PubMed: 8076523]

Moody SA. Fates of the blastomeres of the 16-cell stage *Xenopus* embryo. Dev Biol. 1987a; 119:560–578. [PubMed: 3803718]

Moody SA. Fates of the blastomeres of the 32-cell-stage *Xenopus* embryo. Dev Biol. 1987b; 122:300–319. [PubMed: 3596014]

Moya IM, Alarcon I, del Pino EM. Gastrulation of *Gastrotheca riobambae* in comparison with other frogs. Dev Biol. 2007; 304:467–478. [PubMed: 17306246]

Nakajima K, Yaoita Y. Comparison of TALEN scaffolds in *Xenopus tropicalis*. Biol Open. 2013; 2:1364–1370. [PubMed: 24285709]

Nakayama T, Fish MB, Fisher M, Oomen-Hajagos J, Thomsen GH, Grainger RM. Simple and efficient CRISPR/Cas9-mediated targeted mutagenesis in *Xenopus tropicalis*. Genesis. 2013; 51:835–843. [PubMed: 24123613]

Nieuwkoop, PD.; Faber, J. Normal Table of Xenopus laevis (Daudin): A Systematical & Chronological Survey of the Development from the Fertilized Egg till the End of Metamorphosis. Amsterdam: 1994.

Ogino H, McConnell WB, Grainger RM. High-throughput transgenesis in *Xenopus* using I-SceI meganuclease. Nat Protoc. 2006; 1:1703–1710. [PubMed: 17487153]

Parker HW. Reports of an Expedition to Brazil and Paraguay in 1926–7, supported by the Trustees of the Percy Sladen Memorial Fund and the Executive Committee of the Carnegie Trust for Scotland. Amphibia and Reptilia. J Proc Linn Soc Zoology. 1931:285–289.

Perez OD, Lai NB, Buckley D, del Pino EM, Wake MH. The morphology of prehatching embryos of *Caecilia orientalis* (Amphibia: Gymnophiona: Caeciliidae). J Morphol. 2009; 270:1492–1502. [PubMed: 19572309]

Ramsdell AF, Bernanke JM, Trusk TC. Left-right lineage analysis of the embryonic *Xenopus* heart reveals a novel framework linking congenital cardiac defects and laterality disease. Development. 2006; 133:1399–1410. [PubMed: 16527986]

Rao N, Song F, Jhamb D, Wang M, Milner DJ, Price NM, Belecky-Adams TL, Palakal MJ, Cameron JA, Li B, Chen X, Stocum DL. Proteomic analysis of fibroblastema formation in regenerating hind limbs of *Xenopus laevis* froglets and comparison to axolotl. BMC Dev Biol. 2014:14–32. [PubMed: 24625099]

Romero-Carvajal A, Saenz-Ponce N, Venegas-Ferrin M, Almeida-Reinoso D, Lee C, Bond J, Ryan MJ, Wallingford JB, del Pino EM. Embryogenesis and laboratory maintenance of the foam-nesting tungara frogs, genus *Engystomops* (= *Physalaemus*). Dev Dyn. 2009; 238:1444–1454. [PubMed: 19384855]

Ruibal R, Thomas E. The obligate carnivorous larvae of the frog *Lepidobatrachus laevis* (Leptodactylidae). Copeia. 1988; 3:591–604.

Saint-Jeannet JP, Karavanov AA, Dawid IB. Expression of mesoderm markers in *Xenopus laevis* Keller explants. Int J Dev Biol. 1994; 38:605–611. [PubMed: 7779682]

Sakane Y, Sakuma T, Kashiwagi K, Kashiwagi A, Yamamoto T, Suzuki KT. Targeted mutagenesis of multiple and paralogous genes in *Xenopus laevis* using two pairs of transcription activator-like effector nucleases. Dev Growth Differ. 2014; 56:108–114. [PubMed: 24329851]

Sater AK, Jacobson AG. The specification of heart mesoderm occurs during gastrulation in *Xenopus laevis*. Development. 1989; 105:821–830. [PubMed: 2598816]

Sater AK, Jacobson AG. The restriction of the heart morphogenetic field in *Xenopus laevis*. Dev Biol. 1990; 140:328–336. [PubMed: 2373257]

Scadding SR. Phylogenic Distribution of Limb Regeneration Capacity in Adult Amphibia. J Exp Zool. 1977; 202:57–67.

Sive, HL.; Grainger, RM.; Harland, RM. Early Development of Xenopus laevis. Cold Spring Harbor, New York: Cold Spring Harbor Laboratory Press; 1998.

Smith JC, Symes K, Hynes RO, DeSimone D. Mesoderm induction and the control of gastrulation in *Xenopus laevis*: the roles of fibronectin and integrins. Development. 1990; 108:229–238. [PubMed: 2351067]

Smith WC, Knecht AK, Wu M, Harland RM. Secreted noggin protein mimics the Spemann organizer in dorsalizing *Xenopus* mesoderm. Nature. 1993; 361:547–549. [PubMed: 8429909]

Sobkow L, Epperlein HH, Herklotz S, Straube WL, Tanaka EM. A germline GFP transgenic axolotl and its use to track cell fate: dual origin of the fin mesenchyme during development and the fate of blood cells during regeneration. Dev Biol. 2006; 290:386–397. [PubMed: 16387293]

Spemann H, Mangold H. Induction of embryonic primordia by implantation of organizers from a different species. Roux's Arch Entw Mech. 1924; 100:599–638.

Stuart SN, Chanson JS, Cox NA, Young BE, Rodrigues AS, Fischman DL, Waller RW. Status and trends of amphibian declines and extinctions worldwide. Science. 2004; 306:1783–1786. [PubMed: 15486254]

Sun L, Bertke MM, Champion MM, Zhu G, Huber PW, Dovichi NJ. Quantitative proteomics of *Xenopus laevis* embryos: expression kinetics of nearly 4000 proteins during early development. Sci Rep. 2014; 4:4365. [PubMed: 24626130]

Suzuki KT, Isoyama Y, Kashiwagi K, Sakuma T, Ochiai H, Sakamoto N, Furuno N, Kashiwagi A, Yamamoto T. High efficiency TALENs enable F0 functional analysis by targeted gene disruption in *Xenopus laevis* embryos. Biol Open. 2013; 2:448–452. [PubMed: 23789092]

Tandon P, Showell C, Christine K, Conlon FL. Morpholino injection in *Xenopus*. Methods Mol Biol. 2012; 843:29–46. [PubMed: 22222519]

Tank PW, Carlson BM, Connelly TG. A staging system for forelimb regeneration in the axolotl, *Ambystoma mexicanum*. J Morphol. 1976; 150:117–128. [PubMed: 966285]

Whited JL, Lehoczky JA, Tabin CJ. Inducible genetic system for the axolotl. Proc Natl Acad Sci U S A. 2012; 109:13662–13667. [PubMed: 22869739]

Wilson PA, Oster G, Keller R. Cell rearrangement and segmentation in *Xenopus*: direct observation of cultured explants. Development. 1989; 105:155–166. [PubMed: 2806114]

Woodland HR, Jones EA. The development of an assay to detect mRNAs that affect early development. Development. 1987; 101:925–930. [PubMed: 2903042]

Wuhr M, Freeman RM Jr, Presler M, Horb ME, Peshkin L, Gygi SP, Kirschner MW. Deep proteomics of the *Xenopus laevis* egg using an mRNA-derived reference database. Curr Biol. 2014; 24:1467–1475. [PubMed: 24954049]

Yergeau DA, Johnson Hamlet MR, Kuliyev E, Zhu H, Doherty JR, Archer TD, Subhawong AP, Valentine MB, Kelley CM, Mead PE. Transgenesis in *Xenopus* using the Sleeping Beauty transposon system. Dev Dyn. 2009; 238:1727–1743. [PubMed: 19517568]

Yokoyama H, Maruoka T, Ochi H, Aruga A, Ohgo S, Ogino H, Tamura K. Different requirement for Wnt/beta-catenin signaling in limb regeneration of larval and adult *Xenopus*. PLoS One. 2011; 6:e21721. [PubMed: 21814549]

Young HE, Bailey CF, Dalley BK. Gross morphological analysis of limb regeneration in postmetamorphic adult. Ambystoma Anat Rec. 1983; 206:295–306. [PubMed: 6614512]

Young JJ, Cherone JM, Doyon Y, Ankoudinova I, Faraji FM, Lee AH, Ngo C, Guschin DY, Paschon DE, Miller JC, et al. Efficient targeted gene disruption in the soma and germ line of the frog *Xenopus tropicalis* using engineered zinc-finger nucleases. Proc Natl Acad Sci U S A. 2011; 108:7052–7057. [PubMed: 21471457]

Ziermann JM, Infante C, Hanken J, Olsson L. Morphology of the cranial skeleton and musculature in the obligate carnivorous tadpole of *Lepidobatrachus laevis* (Anura: Ceratophryidae). Acta Zool. 2013; 94:101–112.

Highlights

- Development of the Budgett's frog, *Lepidobatrachus laevis*, as compared to *Xenopus laevis*.
- *L. laevis* embryos are amenable to developmental biology research.
- *L. laevis* embryos are larger than *X. laevis*, yet can develop faster.
- The larger size of *L. laevis* embryos enhances fate mapping and cellular resolution.
- *L. laevis* development has the potential to accelerate biological experimentation.

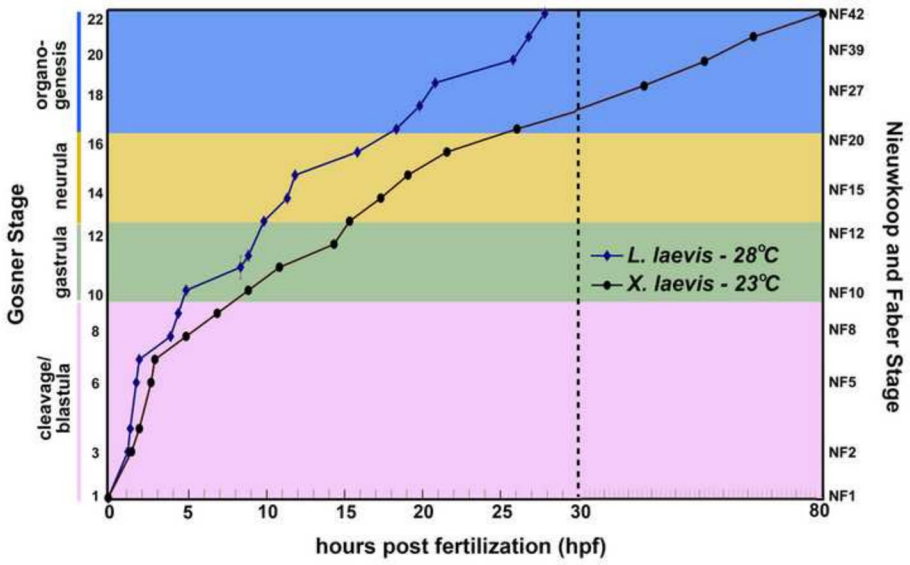

Figure 1.

The schedule of *Lepidobatrachus laevis* embryonic development (versus *Xenopus laevis*). Developmental trajectories from fertilization (Gosner stage 1; GS1) to early tadpole (GS22) were plotted for *L. laevis* (blue diamonds, 28°C) and *X. laevis* (black circles, 23°C). Data points for *L. laevis* were calculated from the average time to achieve the developmental milestones characteristic of each stage in at least three separate clutches of embryos from at least two different adult breeding pairs. Developmental timing of *Xenopus laevis* was plotted from published reports (Nieuwkoop and Faber, 1994). For clarity, stages are clustered into cleavage/blastula (pink), gastrula (green), neurula (yellow) and organogenesis (blue) phases. The dashed line at 30 hpf indicates a break in the x-axis, to accommodate the substantial difference (~50 hours) in the developmental schedule of the two species (at their respective optimal temperatures—note that both organisms develop at the same rate when raised at mutually permissive temperatures; see Figure 5). Gosner (GS) and Nieuwkoop and Faber (NF) stages are indicated.

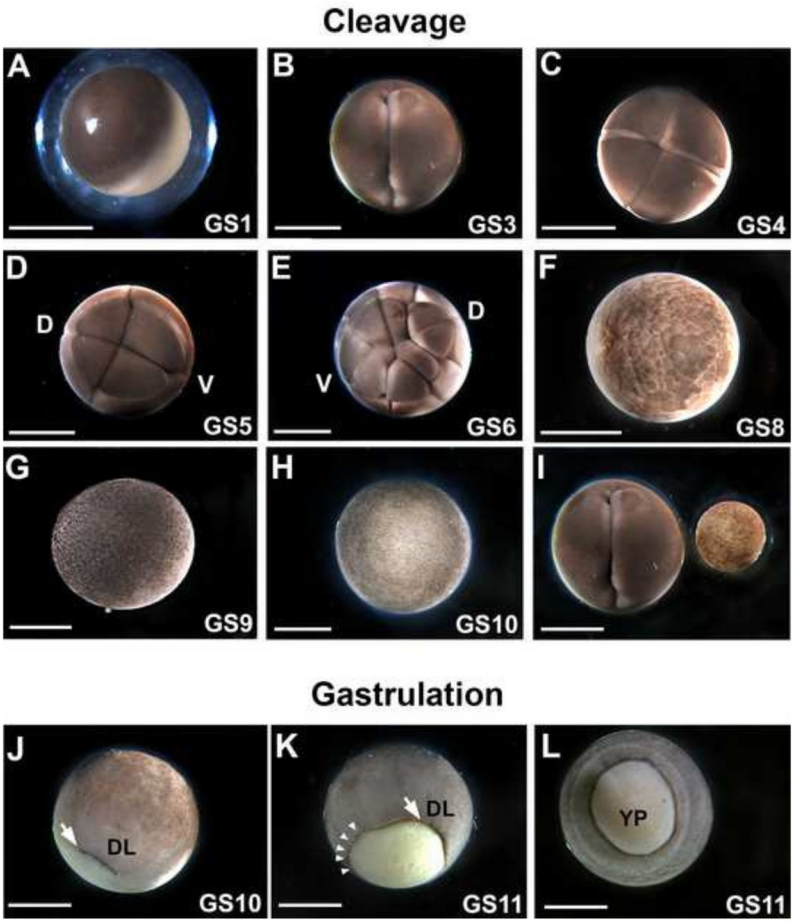

Figure 2.

Early cleavage and gastrulation patterns in *L. laevis* are similar to *Xenopus*. Representative images of *L. laevis* fertilization (A; GS1); 2-cell (B; GS3); 4-cell (C; GS4); 8-cell (D; GS5); 16-cell (E; GS6); mid-blastula (F; GS8); late blastula (G; GS9); and early gastrula (H; GS10). "D" and "V" indicate the prospective dorsal and ventral sides of the embryo, respectively. (I) A side-by-side comparison of a *L. laevis* 2-cell stage embryo with a *X. laevis* gastrula demonstrates the substantial size difference between the two species. J) The dorsal lip (DL) is obvious as a pigmented depression (arrow) in the early gastrula (GS10). K) The dorsal lip (arrow) expands circumferentially (arrowheads). L) The yolk plug is still slightly protuberant in the midgastrula (GS 11). A–I are animal views; J and K are latero-vegetal views; L is a vegetal view. Scale bar = 1 mm.

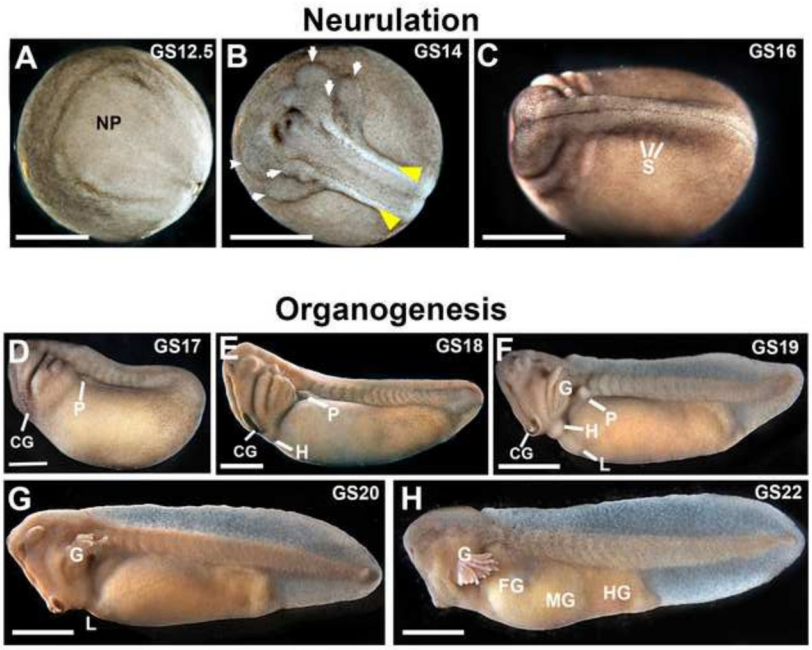

Figure 3.

Neurulation and organogenesis in *L. laevis*. The neural plate (A; GS12.5), neural folds (yellow arrowheads, B; GS14) and migrating streams of neural crest (arrows, B; GS14) are highly prominent in dorsal views of early neurulae. C) Neural tube closure is complete and individual somites (S) are evident by GS16. D-F) The cement gland (CG) and pronephros (P) are visible at the earliest tailbud stages (GS17-19). G–H) Later tailbud stages (GS20-22) show rapid tail elongation, the development of gills and craniofacial features (see also Figure 4), and early gut morphogenesis. NP= neural plate; H=heart; L=liver; G=gills; FG=foregut; MG=midgut; HG=hindgut. Scale bar = 1 mm.

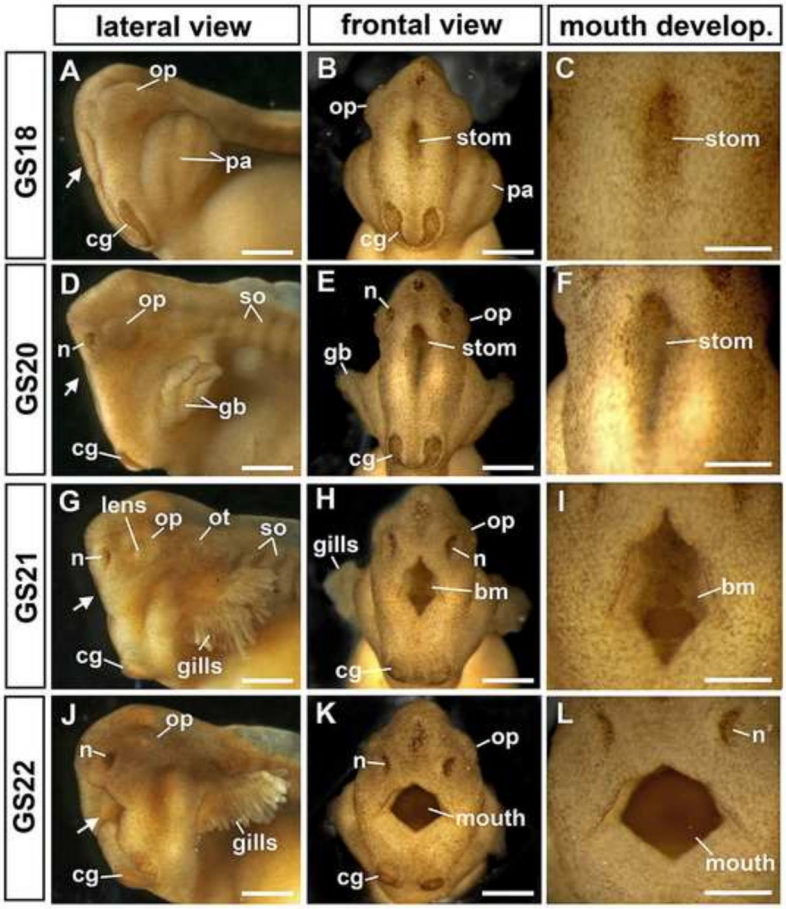

Figure 4.

Craniofacial morphogenesis in *L. laevis*. The embryonic head is shown in lateral (A,D,G,J; anterior to the left) and frontal views (B,E,H,K). Arrows indicate the location of the stomodeum (stom), or mouth. Higher magnification views (C,F,I,L) detail the gradual maturation of the mouth, including the perforating buccopharyngeal membrane (bm). The face and mouth widen dramatically as development proceeds, and the cement gland (cg), which initially forms a horseshoe shape (B), becomes bifurcated as the face widens (K). Gosner Stages (GS) are as indicated. Scale bars in A–B, D–E, G–H and J–K = 500μm; scale bars in C,F,I,L = 250μm. Other abbreviations: gb=gill buds; n=nasal pits; op=optic cup; ot=otic vesicle, pa=pharyngeal arches; so= somites.

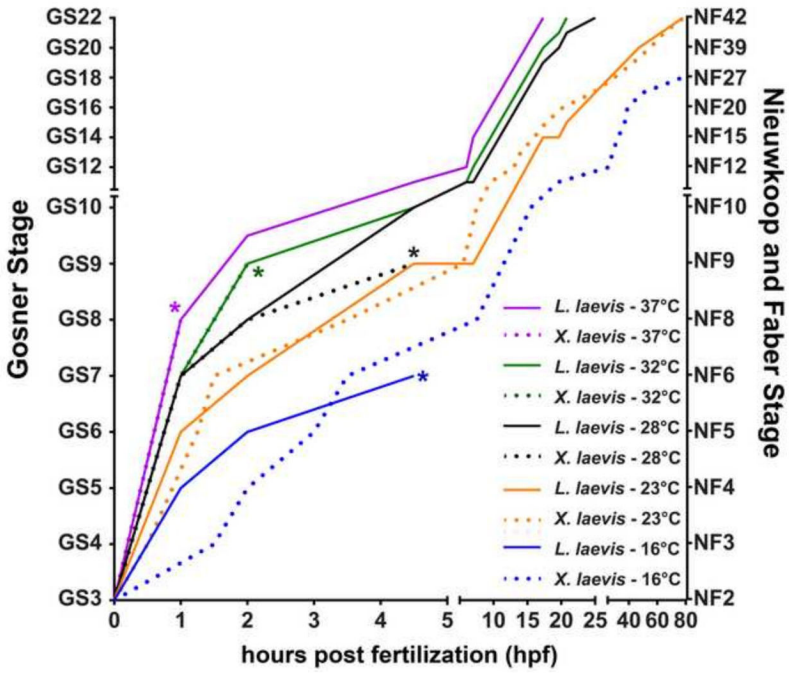

Figure 5.

Thermal tolerance of *L. laevis* and *X. laevis* embryos. *L. laevis* (solid lines, n=10) and *X. laevis* (dotted lines, n=20) were assayed for growth from 2-cell stage (GS3) to tadpole (GS22) at 37°C (purple), 32°C (green), 28°C (black), 23°C (orange), 16°C (blue). Asterisks (*) indicate time points at which at least 50% of embryos fail to gastrulate, indicating decreased viability. Gosner (GS) and Nieuwkoop and Faber (NF) stages are indicated.

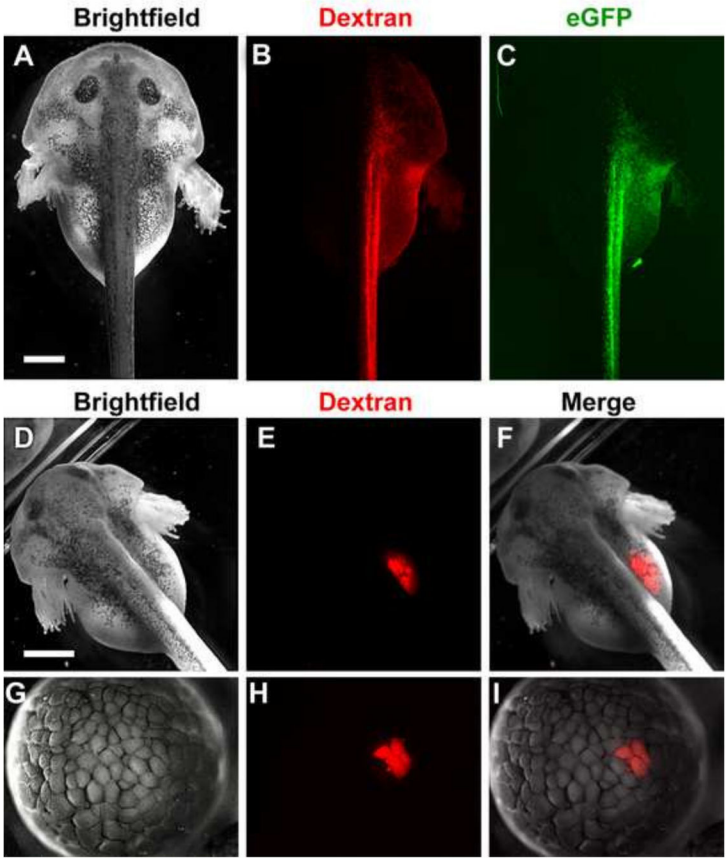

Figure 6.

L. laevis embryos are amenable to microinjection of exogenous reagents for fate-mapping and expression of synthetic mRNA. Embryos were injected at the 2-cell stage (A–C), 8-cell stage (D–F) or 128-cell stage (G–I) with red fluorescent dextran and/or capped *eGFP* mRNA. By 48 hours post fertilization (hpf), injection into a single blastomere at the 2-cell stage results in predominantly unilateral labeling (B) and expression of eGFP (C, green), while injection into a single blastomere at the 8-cell stage results in fluorescence limited to the developing gut (E). Injection of dextran into a single blastomere at the 128-cell stage labels a limited region of only 4 cells by the mid-blastula stage (H). Merge of brightfield and fluorescent images in (F, I). Scale bars = 1 mm.

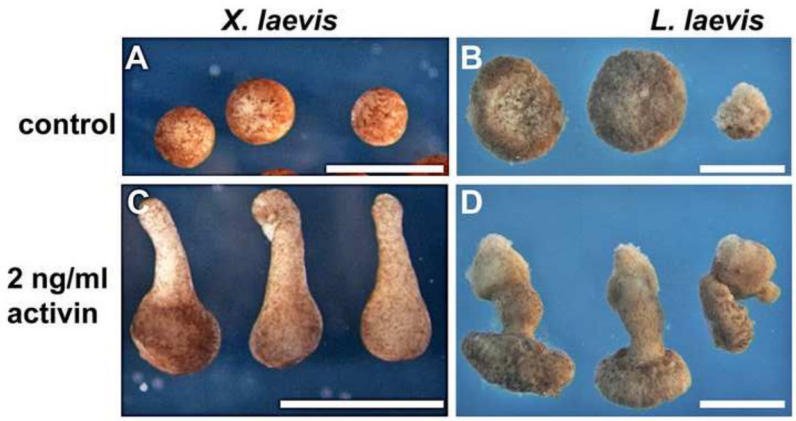

Figure 7.

L. laevis explants are amenable to animal cap explant culture. Untreated animal caps from *X. laevis* (A) or *L. laevis* (B) heal into balls of ciliated epidermis. In contrast, treatment of freshly microdissected caps with activin results in significant elongation of dissected tissue in both *X. laevis* (C) and *L. laevis* (D). The smaller rightmost cap in B and D was trimmed to a reduced size. Scale bars = 1 mm.

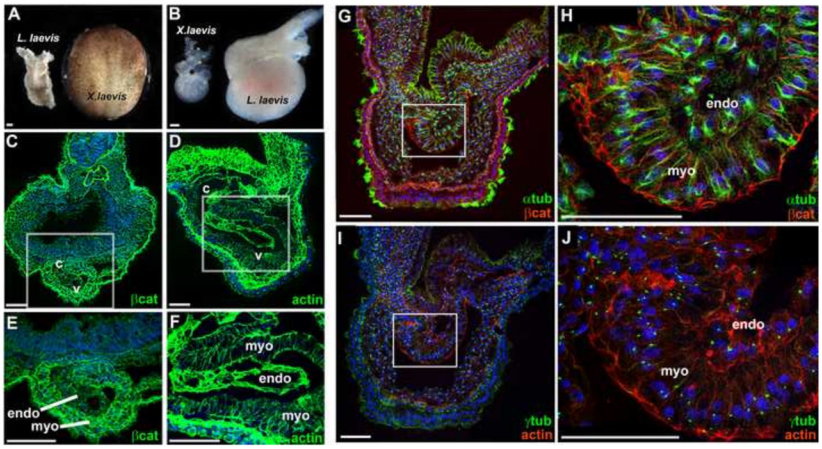

Figure 8.

Heart morphogenesis occurs at a larger scale in *L. laevis*. The scale of *L. laevis* cardiogenesis is illustrated by comparing a dissected *L. laevis* heart tube (GS18) with a whole *X. laevis* neurula embryo (A), and by comparing mature hearts isolated at an equivalent stage from each species (B; GS22). Immunofluorescence analysis of tissue architecture was performed on transverse sections through the heart of GS21 (C–F) and GS20 (G–J) embryos. C–F) Localization of beta-catenin (βcat; green) in *X. laevis* and actin (actin; green) in *L. laevis* reveals the cellular architecture of the heart. G–H) Localization of the microtubule marker alpha-tubulin (αtub; green) and beta-catenin (βcat; red) in the *L. laevis* heart tube. I–J) Localization of the centrosome marker gamma-tubulin (γtub; green), and filamentous actin (F-actin; red), in a neighboring section through the *L. laevis* heart tube. Nuclei are counterstained with TO-PRO-3. White boxes in C, D, G, I indicate regions of the heart magnified in E, F, H, J, respectively. c, conus; v, ventricle; endo, endocardial layer; myo, myocardium. Scale bars = 100 μm.

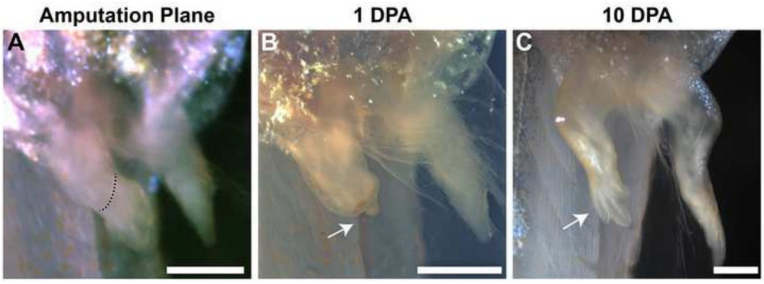

Figure 9.

Limb regeneration occurs at a rapid pace in *L. laevis*. Amputation was conducted on 8-day tadpoles at the indicated level (red dotted line; A). A blastema was identified within 24 hours of amputation (arrow; B). Full regeneration was observed in the operated limb by 10 days post amputation (C).